Cretaceous Research 30 (2009) 1205–1216

Contents lists available at ScienceDirect

Cretaceous Research

journal homepage: www.elsevier.com/locate/CretRes

Paleoclimatic approach to the origin of the coloring of Turonian pelagic limestones from the Vispi Quarry section (Cretaceous, central Italy)

Yuanfeng Cai*, Xiang Li, Xiumian Hu, Xiaoming Chen, Yuguan Pan

State Key Laboratory of Mineral Deposits Research, School of Earth Sciences and Engineering, Nanjing University, Nanjing, 210093, China

ARTICLE INFO

Article history:
Received 9 October 2008
Accepted in revised form 19 June 2009
Available online 30 June 2009

Keywords:
Boehmite
Hematite
Paleoclimate
Mn^{2+}-calcite
Turonian
Pelagic limestone

ABSTRACT

Samples of Turonian white to light gray and red limestones from the Vispi Quarry section in central Italy have been examined by X-ray Diffractometry (XRD), Electron Probe Micro-analysis (EPMA), Electron Spin Resonance (ESR), and Ultra violet-visible-near infrared (UV-VIS-NIR) Diffuse Reflectance Spectroscopy (DRS). The ESR, EPMA and XRD results suggest that Mn^{2+} was well-incorporated into the structure of calcite during the precipitation of the limestones. Amorphous ferric oxide (most probably hematite) and the Mn^{2+}-bearing calcite endowed the limestone with a red color as the major pigmentation, and the Mn^{2+}-bearing calcite gave it a pink tinge. The mineral assemblage is composed mainly of detrital boehmite and quartz, which are interpreted as having been imported from the Eurasian paleo-continent into the ocean by seasonal northeasterly winds. The boehmite formed by dehydration of gibbsite as an end-product of intensive chemical weathering of Fe, Mg, and Al-bearing aluminosilicates exposed in a subtropical environment. XRD results for the residues of Cretaceous Oceanic Red Beds (CORBs) dissolved in dilute acetum differed from those from Cretaceous Oceanic White Beds (COWBs) in that they contain hematite. This suggests that no hematite was imported into the ocean during the precipitation of the white limestone, and may explain why the same detrital origin for red and white limestones resulted in different colors by suggesting that climatic variations occurred on the paleo-continent during the precipitation of these two types of limestone. The presence of boehmite and hematite suggests that, during the Late Cretaceous, central Italy lay within a subtropical climatic zone with a seasonal alternation of warm rainy winters and hot, dry summers during the formation of the CORBs, and a continuously warm climate during the formation of the COWBs. The Mn/Fe(mol) ratios in the shells of spherical carbonate assemblages (probable microfossils) suggested that the ocean was much richer in iron during the precipitation of COWBs.

© 2009 Elsevier Ltd. All rights reserved.

1. Introduction

Hematite pigmentation has been considered to be the most important factor in the formation of the red color in sediments (Van Houten, 1973; Turner, 1980; Franke and Paul, 1980; Pye, 1983; Torrent and Schwertmann, 1987; Einsele, 1992; Eren and Kadir, 1999, 2001). Two hypotheses are usually put forward for the origin of the hematite (Yilmaz, 2008): the first involves the derivation of detrital hematite from lateritic soils while the second involves authigenic precipitation from the weathering of iron-bearing (detrital) minerals such as pyrite, chlorite, biotite, amphibole, pyroxene and olivine. Similar explanations have been suggested for the red pigmentation in limestones (Eren and Kadir, 1999, 2001; Yilmaz, 2008) but there are some red limestones, such as the Upper Cretaceous Red Scaglia Rossa limestone from Gubbio in central Italy (Vannucci et al., 1979; Sighinolfi, 1981; Calderoni and Ferrini, 1984), in which no hematite is detectable by XRD. The source of this red color has been much debated, with the most important and frequently mentioned interpretation being that hematite is present only with a low content, fine particle size, and a random distribution, making it undetectable by XRD (Eren and Kadir, 1999, 2001; Hu et al., 2005, 2009; Yilmaz, 2008).

Mn^{2+}-doped materials have been widely used as optical material to produce different wavelengths of visible light (Li et al., 2006), causing yellow to orange-red, red (Macedo et al., 1999), dull orange and violet cathodoluminescence in Mn^{2+}-doped calcite (Habermann et al., 1998). Thermoluminescence occurred at 620 nm, when the Mn^{2+} returned from the excited state back to the ground state (Medlin, 1963; Macedo et al., 1999).

Boehmite is formed from the dehydration of gibbsite and is one of the main components of Mediterranean-type bauxite (D'Argenio and Mindszenty, 1995; Kloprogge et al., 2002). It is largely restricted

* Corresponding author.
E-mail address: caiyf@nju.edu.cn (Y. Cai).

0195-6671/$ – see front matter © 2009 Elsevier Ltd. All rights reserved.
doi:10.1016/j.cretres.2009.06.002

to subtropical areas (Kloprogge et al., 2002) and has been useful for its paleo-climate significance and as a regional marker of global events (D'Argenio and Mindszenty, 1995).

Gibbsite is today widely present in the soils of tropical areas and is an end-product of aluminosilicate weathering in soils (Jongmans et al., 1994; Nieuwenhuyse, 1996; Mulyanto et al., 1999; Bhattacharyya et al., 2000; Furian et al., 2002; Certini et al., 2006) or rocks (Bates, 1962; Wada and Aomine, 1966; Green and Eden, 1971; Wilke and Schwertmann, 1977; D'Argenio and Mindszenty, 1995; Mulyanto et al., 1999; Samuel and Bruno, 2003; Ziegler et al., 2003; Herrmann et al., 2007). It has been widely used as an indicator for an environment of intense chemical weathering, typical of monsoonal climates in tropical and subtropical areas, in which hot rainy seasons alternate with extended dry periods (Mulyanto et al., 1999; Kloprogge et al., 2002; Samuel and Bruno, 2003; Kleber et al., 2007).

Gibbsite can transform into boehmite from room temperature (Perić et al., 1996) up to 185 °C in a hydrothermal environment (Trolard and Tardy, 1987; Mehta and Kalsotra, 1991) or a much higher temperature up to 300 °C (Perić et al., 1996), with the rate of transformation increasing as the temperature increases (Perić et al., 1996). The boehmite started its dehydration process at 480 °C, and completed its dehydration process at 520 °C (Kloprogge et al., 2002). From the temperature range in which boehmite is stable, it would appear that boehmite can only be stable down to a maximum depth of 24 km in the Earth's crust (using a value of 20 °C/km for the general average geothermal gradient, which ranges from 10–35 °C/km).

The paleoclimate record in the Cretaceous strata has revealed several important Oceanic Anoxic Events or "OAEs" (Schlanger and Jenkyns, 1976). OAEs have attracted attention because of numerous organic-carbon embedding in sediments and the significance of global anoxic events. After the Bonarelli (OAE2) anoxic event in the Late Cenomanian (Upper Cretaceous), the oceanic sedimentation changed from the white (COWB) limestones of the Scaglia Bianca to predominantly red (CORB) limestones of the Scaglia Rossa. Investigations into the red Scaglia Rossa from Gubbio date back to the 1960s (Gratziu and Schiaffino, 1967), and subsequent investigations have focused on the mineralogy (Gratziu and Schiaffino, 1967; Sighinolfi, 1981), sedimentology (Arthur, 1976; Arthur and Fischer, 1977; Wezel, 1979; Alvarez and Montanari, 1988; Lowrie et al., 1990; Hu et al., 2006, 2009), biostratigraphy (Premoli-Silva et al., 1977; Premoli-Silva and Sliter, 1994), paleomagnetism (Alvarez et al., 1977; Lowrie and Alvarez, 1977; Channell et al., 1982), and the petrology and geochemistry (Vannucci et al., 1979; Calderoni and Ferrini, 1984) of these beds. Studies on the mineralogy were relatively rare, but have shown that calcite was the major constituent mineral, with K-feldspar, plagioclase, quartz, magnetite and hydrous iron oxides, and clay minerals also detected as minor mineral constituents (Gratziu and Schiaffino, 1967; Vannucci et al., 1979; Sighinolfi, 1981). No manganese-bearing minerals were detected (Calderoni and Ferrini, 1984). To determine the minor phases acid was usually used to dissolve the carbonate, and in order to accelerate the removal of carbonate the samples were usually milled prior to acidisation. The iron-bearing minerals may, at the same time, have been finely ground, and even become partially amorphous and hence more easily dissolved. The widely used citrate-bicarbonate-dithionite (CBD) method provides an example of how fine, amorphous ferric oxide can be easily dissolved and eliminated from clay mineral assemblages.

In this paper, we have compared mineral compositions, chemical compositions and spectral features of the red limestones with those of the white limestones, and then attempted to interpret the origin of the limestone colorations, their detrital source areas and their geological significance.

2. Materials and analytical techniques

2.1. Materials

Turonian (Upper Cretaceous) limestones were intensively sampled in Vispi Quarry section, which is situated northwest of Gubbio and southeast of Monte Cartria in central Italy. A detailed geological sketch-map and a stratigraphic column with the sample locations can be found in Figs. 1 and 2, as previously published by Hu et al. (2006, 2009). The samples covered the transition from the light gray limestone of the Scaglia Bianca Formation to the reddish-pink limestone of the Scaglia Rossa Formation. This stratigraphic transition occurs within the Upper Cretaceous Turonian Stage within a time span of about 0.8 Ma, based on the 7.4 m/Ma sedimentation rate of Premoli-Silva and Sliter (1994). The reddish-pink Scaglia Rossa limestone has been termed a CORB by Hu et al. (2005), and hence the white to light gray (Cretaceous) Scaglia Bianca limestone can be considered to be a COWB.

2.2. Analytical techniques

The XRD measurements were carried out at the State Key Laboratory of Mineral Deposits Research at Nanjing University using a Rigaku D/max-IIIa diffractometer equipped with a Cu-target tube and a curved graphite monochromator, operating at 37.5 kV and 20 mA. The slit systems were 1° (DS/SS) and 0.3 mm for the RS. Samples were step-scanned from 10° to 100° with a step size of 0.02° (2θ). A side-packing method proposed by National Bureau of Standards (NBS) was used to prepare the XRD samples. The quantitative mineral phase analysis and cell parameter refinement were achieved by means of Whole-Pattern Fitting with a General Structural Analysis System (GSAS, Larson and Von Dreele, 2004).

The Electron Spin Resonance (ESR) spectra were recorded at 293 K and 9.76 GHz with an X-band Brücker ER 200 spectrometer using randomly orientated powders, in the Morden Analysis Center at Nanjing University. Equal amounts (100 mg) from each sample were placed in pure silica tubes for a quantitative comparison between the samples.

The Electron Probe Micro-Analysis (EPMA) was carried out using a JOEL JXA-8100 Electron Probe Micro-analyzer at the State Key Laboratory of Mineral Deposits Research in Nanjing University. The instrument was operated at a 15 kV acceleration voltage with a 20 nA beam current. Both plane analyses and chemical analyses were

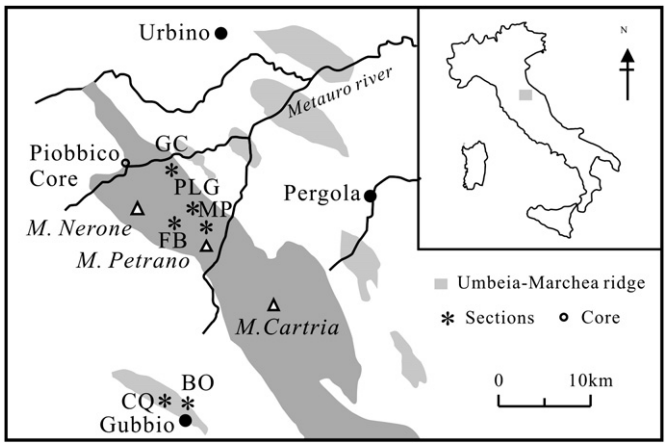

Fig. 1. Location of the studied sections near Gubbio-Piobbico area, the Umbria–Marche Basin, central Italy (modified from Baudin et al., 1998). Sections: BO: Bottaccione Gorge section; CQ: Vispi Quarry section; FB: Fiume Bosso section, GC: Gorgo a Cerbara section; MP: Monte Petrano section; PIO: Piobbico core; PLG: Poggio le Guaine section.

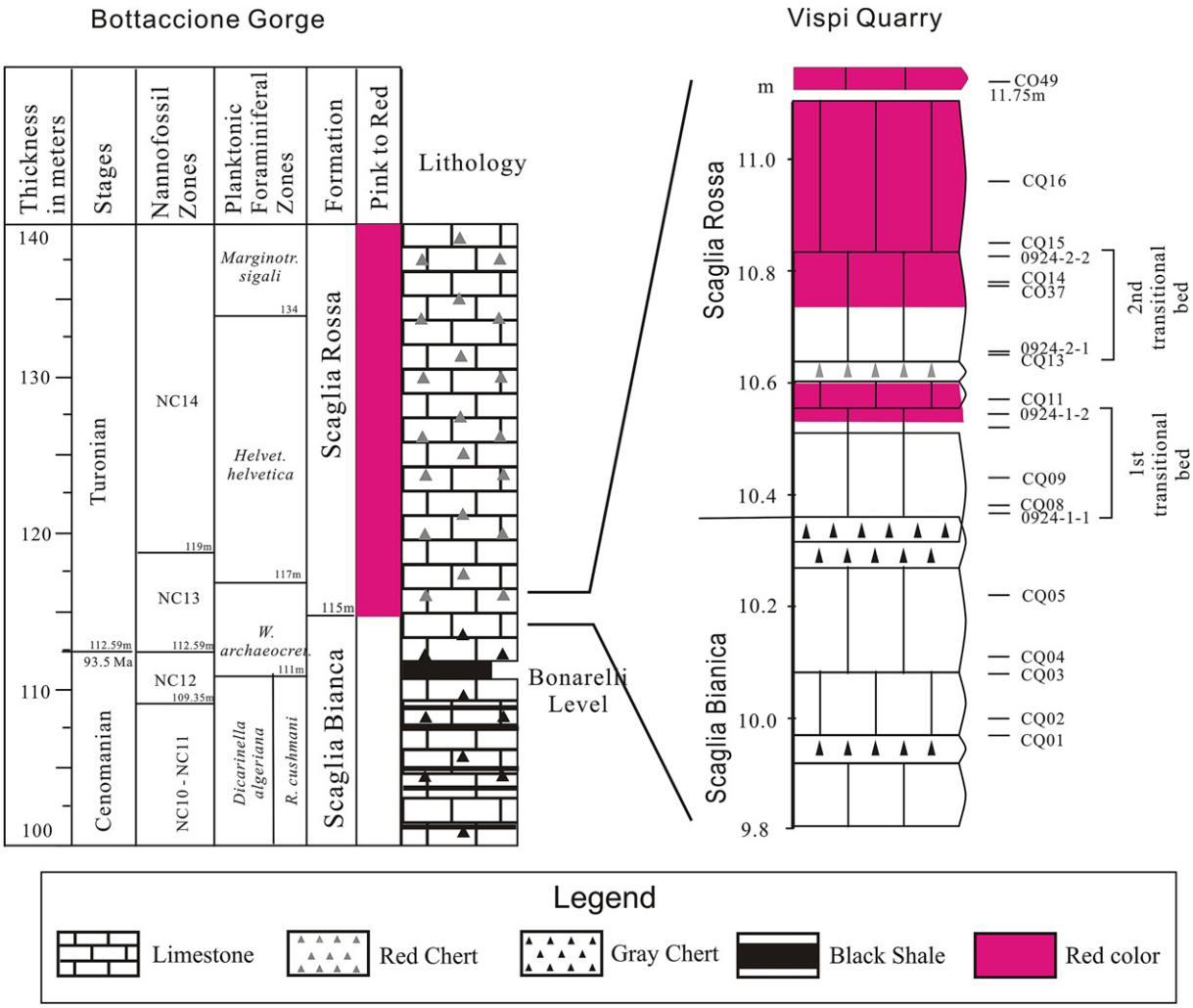

Fig. 2. Detailed lithologic column from the Scaglia Bianca to Scaglia Rossa in the Vispi Quarry section, showing sample positions (right). Left: stratigraphic column from the Upper Cenomanian to the Turonian of the reference Bottaccione Gorge section, showing nannofossil and planktic foraminiferal zones (Premoli-Silva and Sliter, 1994; Tremolada, 2002).

completed. The beam diameter was narrowed to less than 1 μm for the chemical analyses. An amphibole natural mineral standard was used to collect the weight fractions for SiO_2, Al_2O_3, TiO_2, MgO, FeO, Na_2O, and K_2O, while fayalite was used for MnO and calcite for CaO; all of these mineral standards were from the National Institute of Standards and Technology (NIST), U.S.A.

3. Geological setting and lithologies

The Cretaceous pelagic sequence of the Umbria-Marche Basin was deposited near the continental margin of the Apulia block. The block shifted northwards from Africa relative to northern Europe and was strongly affected by pre-orogenic deformation, such as extensional normal faulting (Marchegiani et al., 1999). The basement of the Umbria–Marche Apennines is continental, with the Upper Jurassic through to lower Miocene pelagic strata overlying a Triassic to Lower Jurassic carbonate platform. During the latest phase of the Alpine–Himalayan orogeny in Miocene time (see Centamore et al., 2002), the basin was involved in tectonic compression and became part of the foreland fold-and-thrust belt of the Umbria–Marche Apennines of central Italy. The direction of movement of the thrust sheets was from the southwest towards the northeast.

Since the first pioneering work on biostratigraphy in 1936 (Renz, 1936), detailed studies of type sections at the Vispi Quarry and Bottaccione Gorge have been published frequently (Luterbacher and Premoli-Silva, 1962; Premoli-Silva, 1977; Premoli-Silva and Sliter, 1994; Coccioni et al., 1987, 1989, 1990, 1995; Tremolada, 2002; Coccioni and Luciani, 2004; Hu et al., 2006, 2009).

The Vispi Quarry section forms part of the Cretaceous sedimentary succession outcropping in the Umbria-Marche Basin. The Umbria-Marche succession has been subdivided into four formations on the basis of color changes, carbonate content and the presence or absence of chert and black shales (see Arthur and Fischer, 1977; Alvarez and Montanari, 1988; Coccioni, 1996). The four formations are: the Maiolica Formation (upper Tithonian-lower Aptian), the Marne a Fucoidi Formation (lower Aptian–upper Albian), the Scaglia Bianca Formation (upper Albian-lowest Turonian) and the Scaglia Rossa Formation (lowest Turonian to middle Eocene). The latter two formations have been the subject of this research. The studied section started above the Bonarelli (OAE2) Level, from 9.8 m in the Scaglia Bianca Formation and terminated at 10.9 m in the Scaglia Rossa Formation. Two transitional beds were present, at 10.35–10.55 m and at 10.63–10.83 m, each overlain by completely reddish-pink colored beds (Fig. 2).

The Scaglia Bianca Formation is comprised of yellowish-gray to grayish limestones intercalated with a few pink to reddish

limestone beds and several greenish-gray to black marlstones and shales. The formation has been subdivided into four discrete informal lithologic members (Coccioni et al., 1992). The Bonarelli horizon (OAE2) is a prominent marker bed near the top of the Scaglia Bianca Formation. It is an ichthyolithic–bituminous–radiolarian unit about 1 m thick, consisting of siliceous, carbonate-free olive-green to black mudstone and black shales with more than 23% organic carbon (Arthur and Premoli-Silva, 1982). The Upper Cretaceous Scaglia Rossa Formation has been described in detail by Arthur and Fischer (1977) and Alvarez and Montanari (1988): it is comprised predominantly of pinkish-red marly limestones that generally contain 65–92% $CaCO_3$, except for rare shaly interbeds which accentuate the bedding.

4. Results

4.1. ESR spectral study

Fig. 3 shows the ESR (Electron Spin Resonance) spectra for seven of the eighteen limestone samples. Six hyperfine splitting peaks were present in each of the spectra, suggesting that manganese was present as a divalent cation and well-incorporated into the structure by the replacement of calcium in calcite. This implied that the Mn^{2+} cations remained isolated and hence had no effect on each other, and that the homogenous distribution of Mn^{2+} did not result in an ordered structure like dolomite.

4.2. XRD study

Fig. 4 illustrates eight of the nineteen XRD patterns. These XRD patterns suggested that the mineral phases present in the CORBs from the Scaglia Rossa Formation were the same as those in the gray or white limestones of the Scaglia Bianca Formation. The main minerals were calcite, quartz and boehmite. After the removal of carbonates, montmorillonite and illite were detected in the residues; minor hematite was also detected in the CORBs residues.

Quantitative phase analyses and cell parameter refinements were carried out for three mineral weight fractions by means of whole pattern fitting for eighteen powder XRD patterns. The refined value for a_0 and c_0 were slightly smaller than the calcite (47–1743) listed in the Powder Diffraction File-2 (PDF-2; ICDD, 2004) database. The average, maximum and minimum a_0 and c_0 values were 0.4987196 nm and 1.7054171 nm, 0.498839 nm and 1.7059799 nm, 0.4984934 nm and 1.7046541 nm respectively. The a_0 and c_0 values for calcite (47–1743) were 0.49896 and 1.7061 nm respectively. This might indicate that the Mn^{2+} has replaced part of the calcium in the CaO_6 octahedron.

4.3. EPMA study

4.3.1. Plane analysis for limestone

Five EPMA (Electron Probe Micro-Analyzer) plane analyses were carried out on two pink and one white limestone samples. Figs. 5A, 5B, and 5C illustrate the analysis results for the spherical carbonate (possible micro-fossil), the calcite microlites and the detrital material in the pink limestone (sample 0924-2-2) respectively. Figs. 5D and 5E show the analysis results for samples CQ-37 (pink limestone) and CQ-13 (white limestone) respectively. The distribution of manganese is homogeneous in three of the samples. Iron is homogeneously distributed in the spherical carbonate, the calcite microlites, and in the matrix of the three limestones, but is extremely enriched in the CORBs detrital material, although detrital material was seldom found in CORBs examined by optical microscope. The silicon component was also high in the detrital material where it was mainly present as quartz, but also in montmorillonite and illite.

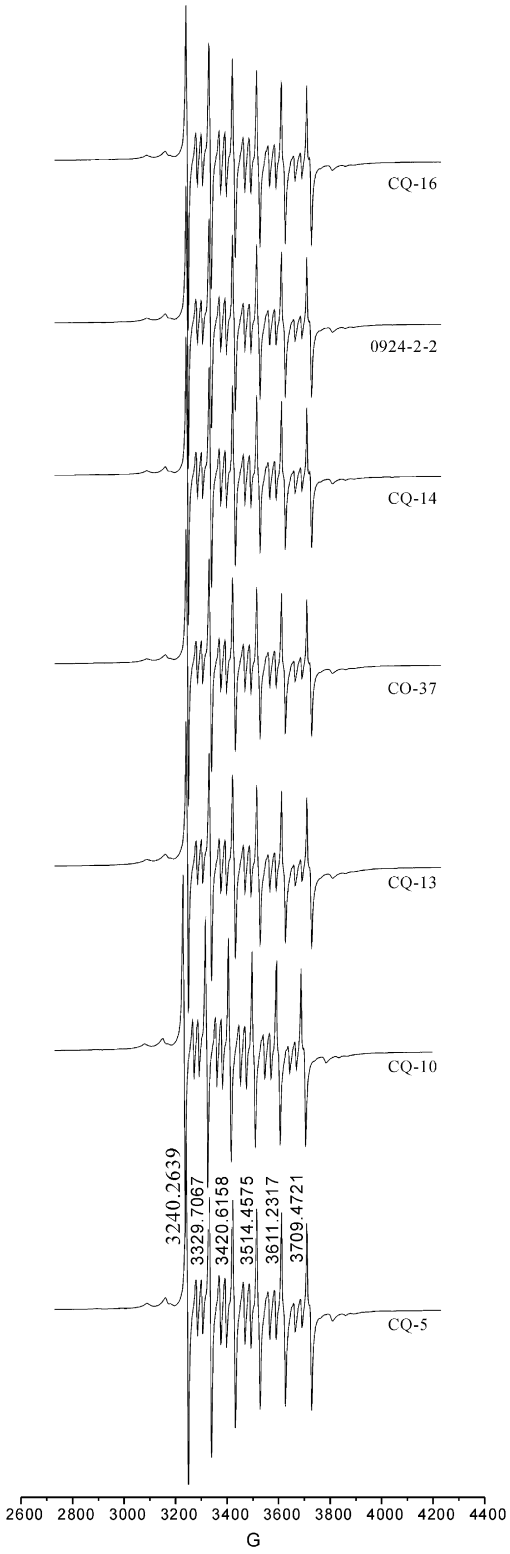

Fig. 3. ESR spectra for selected CORBs and COWBs.

4.3.2. Point analysis for limestone

As illustrated in Fig. 5A, a spherical carbonate (probable microfossil) was present in the limestone; this was made up of a shell-

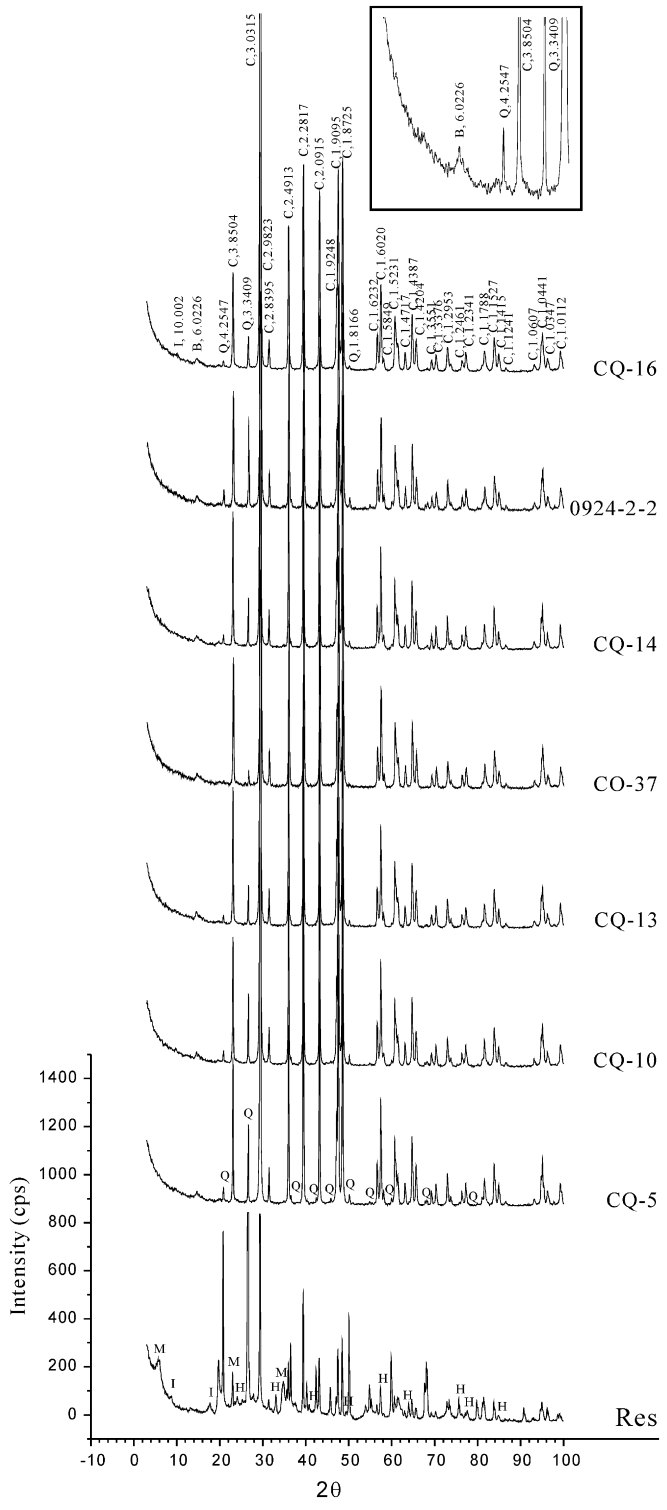

Fig. 4. XRD patterns for selected CORBs and COWBs. In figure: the signs are abbreviations of the mineral: B-boehmite; C-calcite; H-hematite; I-illite; M-montmorillonite saturated with calcium ions; Q-quartz. Res-residue dissolved by the dilute acetum.

like structure with a core and a curved gap between the shell and core, filled with loose material (Fig. 5B). The EPMA chemical analysis for the 0924-2-2 and CQ-37 pink limestone samples and for the CQ-13 white limestone sample are listed in Table 1(1–3). The analyses were carried out on the shell, the filling within the spherical carbonate shell, the film (or epithelial) filling, the matrix and the calcite crystals. Table 1(1–3) shows that the manganese component, as tested at the five points mentioned above, was similar in all three samples. However, the iron content was quite different and was lowest in the spherical carbonate shell from the CORBs. The atomic ratio of $Mn/Fe_{(mol)}$ was therefore used to illustrated the differences between the three samples. The $Mn/Fe_{(mol)}$ ratio for the shells from the pink limestone was much larger than the ratio for the matrix of the white limestone. However, the $Mn/Fe_{(mol)}$ ratio for the matrix of pink limestone was slightly smaller than the ratio for the matrix of the white limestone. It can also be seen from Table 1(1–3) that the $Mn/Fe_{(mol)}$ ratios for the calcite crystal, the epithelial and the filling in the shells were much smaller than the ratios for the shells themselves and the matrix in the pink limestone. However, their $Mn/Fe_{(mol)}$ ratio was similar to the ratio for the shells in the white limestone.

4.3.3. Uv-Vis-NIR spectra study

The Uv-Vis-NIR diffuse reflectance spectra are illustrated in Fig. 6. One broad absorption band centered at about 560 nm and range from 520 to 600 nm, is present in all seven red limestone spectra. This broad absorption of blue-green light results in the strong, bright red of the limestones. A shaded red area at about 575 nm, displayed as one weak peak or shoulder, may be resulted from the presence of Mn^{2+} bearing calcite or crystalline hematite. A detailed DRS study of limestone samples from the Vispi Quarry section can also be found in Hu et al. (2009). The first-derivative spectra of the red and pink limestones showed that there was a prominent peak centered within the 560–570 nm range, and the presence of finely dispersed hematite was suggested. However, no peak was present in the 560–570 nm range in the DRS spectra of the white limestones.

5. Discussion

5.1. Mineralogical and chemical features of the limestones

Apart from calcite, the minor mineral constituents previously identified in the sequential leaching residues were mainly K-feldspar, plagioclase, quartz, and clay minerals (Vannucci et al., 1979); traces of magnetite and hydrous Fe oxides were also detected (Sighinolfi, 1981), but no aluminum or manganese bearing minerals were detected in the Scaglia Rossa samples. According to our XRD results illustrated in Fig. 4, however, boehmite and quartz were the main minor mineral phase. Furthermore, the diffraction line at about 0.611 nm is broad and weak, and there are two much weaker diffraction lines near 0.611 but at high 2θ side illustrated in the upper. It has been suggested therefore that the amount of boehmite present may have been quite small and that it was either poorly crystallized or in an amorphous aluminous oxide state. After the calcite had been dissolved by dilute acetum, montmorillonite and illite were present in the residues, and hematite was also detected in the CORBs. However, the intensity of the boehmite diffraction profile was still very weak and even difficult to identify. It is suggested that the milling decreased the grain size of the boehmite resulting in its dissolution in the dilute acetum. The amorphous iron oxide may also have been similarly affected. The suggestion that boehmite was originally present and subsequently dissolved may also be supported by the reported existence of more than 80% Al (wt%) in the sequential leaching residue of the red carbonate (Calderoni and Ferrini, 1984).

Comparing the chemical compositions for ferric and ferrous iron as measured by EPMA, by combined XRF and by wet chemical analysis and illustrated in Table 1(1–3), the EPMA results differed from the XRF results in their much lower SiO_2, Al_2O_3, TFeO, K_2O, and MgO content. This may suggest that these components were

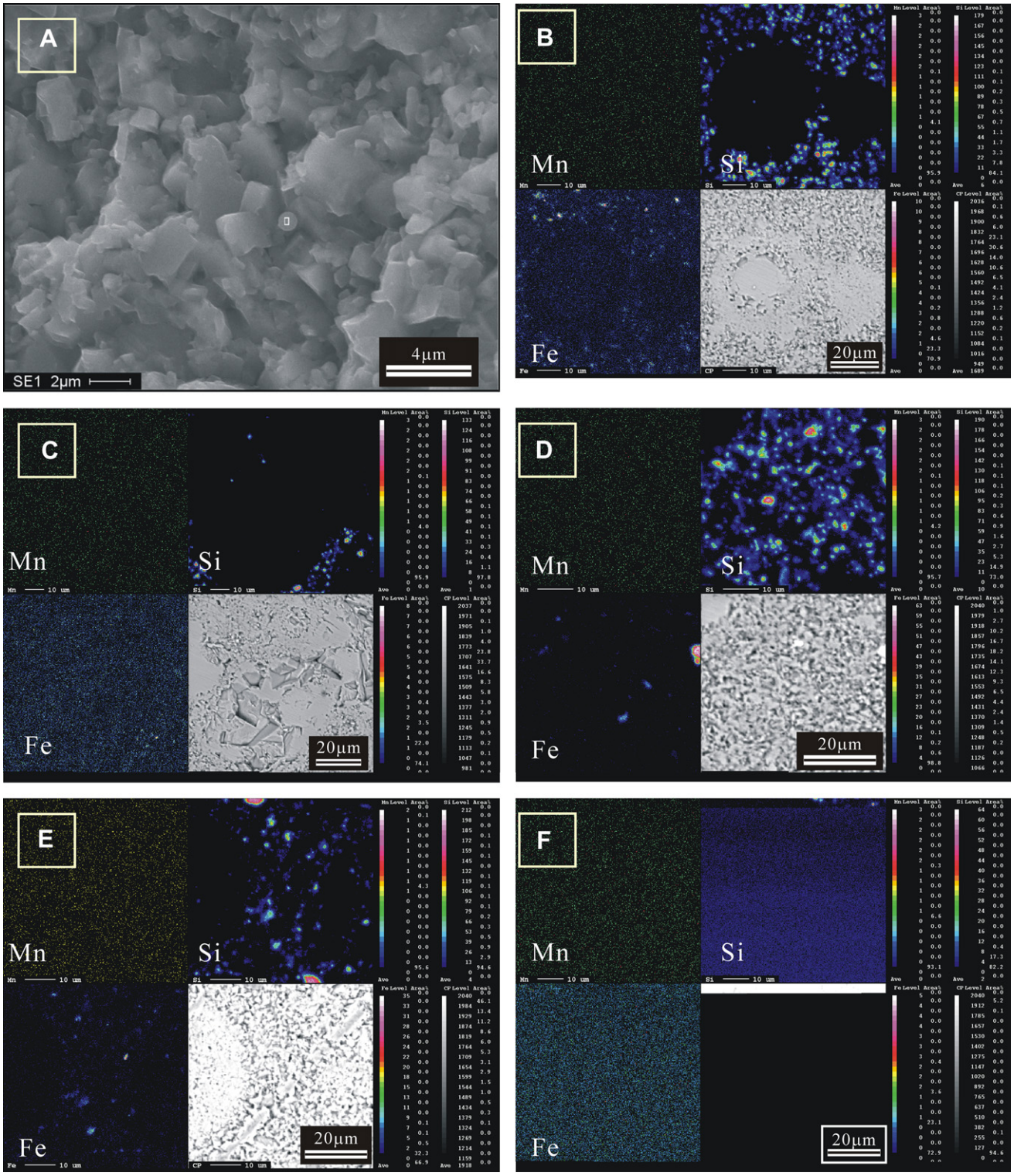

Fig. 5. EPMA plane analyses for two CORBs and one COWB from the Vispi Quarry, Italy. A, SEM image of the spherical carbonate (possible micro-fossil); B, C, D, plane analyses for pink limestone 0924-2-2; E, plane analysis for pink limestone CO-37; F, plane analysis for white limestone CQ-13.

imported into the ocean from the paleo-continent: it should be noted that the total iron oxide measured by EPMA is much smaller than that measured by XRF, but similar to the FeO component obtained by wet chemical analysis, and it can therefore be assumed that the iron measured by EPMA was derived from within the calcite structure and was ferrous iron. This may then suggest that the importation of amorphous ferric oxide or hematite was the reason for the higher ferric oxide component in the CORBs than in the COWBs.

5.2. Distribution of iron and manganese in the limestones

The distribution of manganese was shown by the ESR, XRD, and EPMA plane analysis results as well as previously published

Table 1
EPMA analyses for two CORB limestones and one COWB limestone. (1). EPMA analysis for 0924-2-2 pink limestone. (2). EPMA analysis for CQ-37 pink limestone. (3). EPMA analysis for CQ-13 white limestone

Oxide	Spherical carbonate		Film (7 points)	Matrix (11 points)	Crystal (2 points)	Average (36 points)	XRF Hu et al.,
	Shell (6 points)	Core (10 points)					
SiO_2	0.00	0.00	0.00	0.00	0.00	0.00	5.394
TiO_2	0.015	0.018	0.024	0.024	0.019	0.024	0.020
Al_2O_3	0.034	0.012	0.008	0.016	0.010	0.027	0.561
Fe_2O_3	–	–	–	–	–	–	0.350
FeO	0.015	0.102	0.099	0.058	0.098	0.087	0.063
MnO	0.033	0.053	0.073	0.070	0.053	0.059	0.060
MgO	0.076	0.129	0.161	0.052	0.023	0.105	0.409
CaO	56.584	56.075	56.131	56.201	56.261	56.077	52.030
Na_2O	0.039	0.027	0.019	0.015	0.008	0.024	0.030
K_2O	0.007	0.010	0.004	0.010	0.008	0.008	0.154
Total	56.794	56.379	56.498	56.386	56.454	56.358	
Mn/Fe*	2.172	0.521	0.747	1.222	0.545		–
Oxide	Spherical carbonate		Film (4 points)	Matrix (5 points)	Crystal (0 points)	Average (20 points)	XRF Hu et al.,
	Shell (6 points)	Core (5 points)					
SiO_2	0.00	0.00	0.00	0.00	–	0.00	1.795
TiO_2	0.018	0.002	0.028	0.017	–	0.018	0.017
Al_2O_3	0.015	0.010	0.018	0.025	–	0.016	0.307
Fe_2O_3	–	–	–	–	–	–	0.120
FeO	0.023	0.139	0.125	0.072	–	0.097	0.130
MnO	0.041	0.063	0.064	0.098	–	0.073	0.064
MgO	0.074	0.184	0.149	0.119	–	0.133	0.390
CaO	56.578	56.262	56.032	56.758	–	56.390	54.513
Na_2O	0.044	0.049	0.016	0.016	–	0.026	0.030
K_2O	0.009	0.004	0.009	0.015	–	0.010	0.108
Total	56.737	56.664	56.404	57.087	–	0.097	–
Mn/Fe*	1.834	0.459	0.519	1.377		56.704	–
Oxide	Spherical carbonate		Film (5 points)	Matrix (6 points)	Crystal (1 points)	Average (24 points)	XRF Hu et al.,
	Shell (6 points)	Core (6 points)					
SiO_2	0.00	0.00	0.00	0.00	0.00	0.00	2.399
TiO_2	0.046	0.041	0.004	0.019	0.021	0.030	0.011
Al_2O_3	0.009	0.018	0.019	0.045	0.015	0.024	0.187
Fe_2O_3	–	–	–	–	–		0.020
FeO	0.188	0.126	0.200	0.095	0.086	0.145	0.140
MnO	0.066	0.074	0.087	0.150	0.037	0.087	0.098
MgO	0.130	0.150	0.160	0.110	0.119	0.134	0.329
CaO	56.097	56.181	56.047	56.132	56.112	56.124	54.631
Na_2O	0.034	0.015	0.038	0.032	–	0.030	0.020
K_2O	0.007	0.002	0.016	0.016	–	0.012	0.086
Total	56.473	56.543	56.531	56.528	56.39	56.512	–
Mn/Fe*	0.358	0.596	0.443	1.602	0.436		–

"Mn/Fe*" means the ratio is the mole ratio. "–" not measured.

literature (Calderoni and Ferrini, 1984) to be homogeneous, and it was incorporated into the calcite structure during its formation. The EPMA plane analysis results showed that the manganese is homogeneously distributed in the matrix, the spherical carbonate (micro-fossils) and the calcite microlites. The majority of the manganese was, however, shown to have been associated with the carbonates since, on average, 93.7% of the manganese was leached out concomitantly with the dissolving of the carbonate (Calderoni and Ferrini, 1984).

The distribution of iron was much more complex than that of manganese. Iron was present as lattice iron, iron oxide clustered in the structure, and iron oxide adsorbed on boehmite (or quartz). The EPMA results suggested that the iron was distributed in two different ways. Part of iron was distributed quite homogenously within the matrix, the micro-fossils, and the calcite microlites, suggesting that this form of iron was lattice iron introduced into the crystal structure during the formation of the limestone. Highly concentrated iron was only found in the detrital material (Figs. 3D and 3E), suggesting that iron oxide was adsorbed onto, and transported by, boehmite or quartz. This interpretation was supported by the change in TFe_2O_3 and was closely related to Al_2O_3 (Hu et al., 2009). The presence of iron as clusters within the calcite structure could be assumed from the transformation from iron-bearing calcite. Calderoni and Ferrini (1984) suggested that the majority of the iron was present in detrital fragments since about 80.2%, 4.4% and 15.4% of the iron was present in the residua, the reducible fraction and the carbonate respectively and no more than 4.4% of the iron present was ferric oxide, contributing less than 0.013% to the total 0.29% of iron.

5.3. Contributions of Fe and Mn to mineral color

The color of the sediments or minerals is the result of partial absorption or reflectance of visible light. Absorption in the range of 490–500, 500–560, and 560–580 nm endowed the minerals with red, amaranth, and violet colors, respectively, suggesting that absorption must have occurred within the 490–580 nm range to endow the limestone with its red color.

Hematite has not only been considered the most important source of pigment for the red color in sediments, but also a most important indicator of environmental and paleoclimatic change. Visible Diffuse Reflectance Spectroscopy has proved the most efficient approach for the detection of hematite and has been used for quantitative measurements of hematite content. It is able to detect

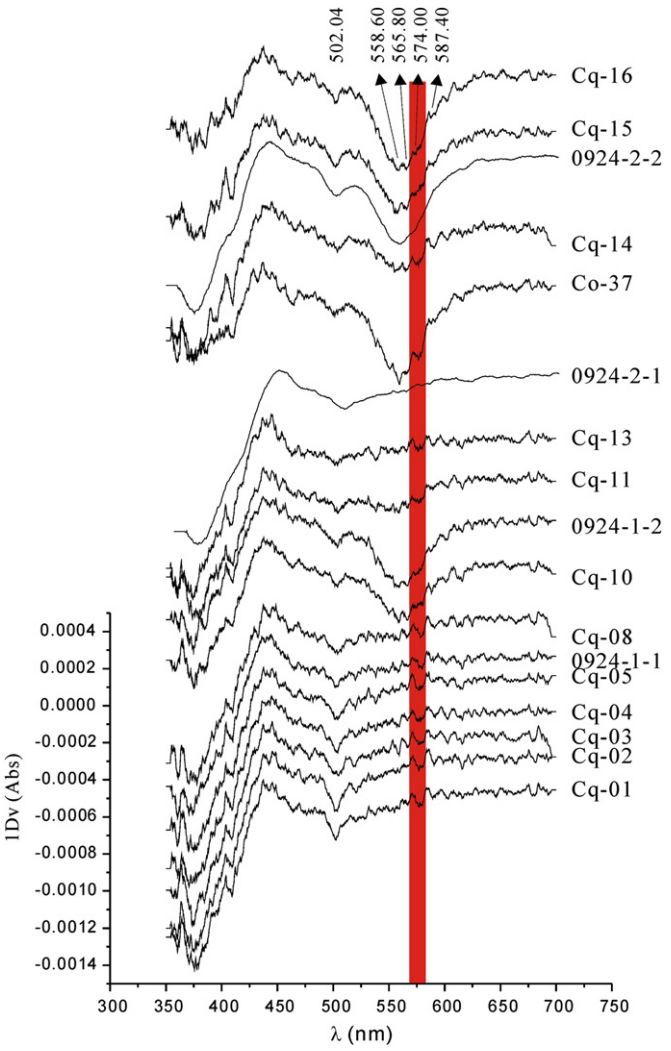

Fig. 6. DRS for CORBs and COWBs.

hematite concentrations as low as 0.05% and 0.01% in mixtures which have a matrix of loess and periclase (Deaton and Balsam, 1991; Ji et al., 2007; Cai et al., 2008). A reflectance peak centered within the 565–575 nm range has been assigned to hematite (Deaton and Balsam, 1991; Ji et al., 2007; Hu et al., 2009), and the peak shifts to a higher wave-number (up to 586 nm) for specularite (Cai et al., 2008). The shifting of the peak can be attributed to an increase in the degree of crystallization. The intensity of the peak centered at 586 nm in the first derivative DRS spectrum is an order of magnitude lower than that for the hematite of sedimentary origin (Cai et al., 2008), which suggests that crystalline hematite such as mica hematite or specularite has a much lower dyeing potential than the amorphous or weakly crystalline hematite. This is supported by the degree of dyeing observed on the inner wall of the agate mortar used during the hematite milling: no dyeing was observed during the milling of specularite or mica hematite, but the hematite of sedimentary origin dyed the wall a red color that was difficult to remove, even by washing with a dilute acid solution. More importantly, however, there was a rhodochrosite peak centered at 577 nm in the DRS (Cai et al., 2008). As is well known, rhodochrosite, as well as Mn^{2+}-bearing calcite and other Mn2+ bearing silicate minerals, have a bright, transparent to translucent red color. Hence, the peak centered in the range of 565–575 nm can not on its own be taken as evidence for the presence of hematite, especially in Mn^{2+} bearing limestone, and the presence of hematite should therefore be confirmed by both XRD and wet chemical analysis as a prerequisite, in order to exclude the presence of Mn^{2+}-calcite. The XRD results for the residues from dilute acetum dissolution suggested that hematite was present in the CORBs and might therefore be responsible for its red color.

5.3.1. The coloring mechanism of iron oxide

A common theory for the coloring effect of iron oxides is that it is due to the presence of very fine and homogeneously distributed particles within the rocks or sediments. This theory is easily understood and has been used to explain the coloring mechanisms for several kinds of rock loess and soil (Deaton and Balsam, 1991; Ji et al., 2007), including red detrital sedimentary rocks, hematite-cemented sedimentary rocks, and granite (Putnis et al., 2007). It is, however, very difficult to prove, especially if the distribution of hematite is inhomogeneous, or if it can not be detected.

The iron originally entrapped in the calcite structure can have one of two species, the first of which is ferrous iron and constructing the calcite structure, and the second of which is iron found in the interstices of the calcite structure which spoliates the oxygen from the CaO_6 octahedron to form $Fe_2O_3^{2-}$ clusters. These clusters can then be oxidized to form hematite clusters by releasing the electron to O_2 dissolved in groundwater. These hematite clusters can grow to several tens of nanometers within the structure of the calcite, and could therefore be another coloring factor, endowing the limestone with a homogeneous red color.

5.3.2. The coloring mechanism of manganese

The ESR spectra for the limestones clearly show that manganese is present as octahedral cations within the calcite structure. Although Mn^{2+}-bearing calcite and rhodochrosite are known to have a red color, this was significantly lighter after the rhodochrosite had been ground to a powder than it had been in the crystals, which suggests that Mn^{2+}-bearing calcite with a fine particle size may only give the limestone a light red tinge. The color may only be detected by DRS as the Mn^{2+} concentration within the structure can be very low.

Mn^{2+}-doped calcite can be excited to radiate visible red light by means of thermal, cathodoluminescent, ultraviolet or laser energy sources. This effect has been attributed to the Mn^{2+} returning from an excited state back to the ground state (Medlin, 1963; Habermann et al., 1998; Macedo et al., 1999; Li et al., 2006). A similar mechanism may also affect the Mn^{2+} incorporated into the structure of calcite in Mn^{2+}-bearing limestones. The Mn^{2+}-bearing calcite, which was comprised of both pale pink to purple-red calcite and white calcite, outcropped in a different location within a uranium bearing deposit. The pale pink to red calcite outcropped close to uraninite whereas the white calcite was further away, so that the red color might be attributable to radiation from the decay of uranium (Zhang et al., 2005). The uranium and thorium contents were analyzed by ICPMS (Hu et al., 2009) and ranged between 0.08–4.92 ppm for uranium (average 0.62) and 0.24–0.37 ppm for thorium (average 0.28) in the CORBs, compared to 0.06–1.54 ppm for uranium (average 0.29) and 0.16–0.39 for thorium (average 0.26) in the white limestone. The γ-radiation that accompanies the isotope decay from U to Pb and Th to Pb may therefore have provided the required energy source for the red coloration.

5.4. Distribution of terrestrially derived detrital matter and its geological significance

5.4.1. Major and trace element variations within the section

Both the major element analyses and the quantitative phase analyses from XRD showed that the limestone samples were composed mainly of calcite ($CaCO_3$). The quantitative phase

Table 2
Geochemical parameters of the different sediment groups at Vispi Quarry section, Gubbio, Italy

Element oxide	Scaglia Rossa (Red) $N=8$			Scaglia Rossa (white) $N=5$			Scaglia Bianica1 $N=5$			Scaglia Bianica (above) 2 $N=73$		
	Conc. (1 d, max)	−/Al (1d)	EF	Conc. (1 d, max)	−/Al (1d)	EF	Conc. (1 d, max)	−/Al (1d)	EF	Conc. (1 d, max)	−/Al (1d)	EF
SiO_2	3.19 (1.21, 5.39)	1.49(0.57)	1.83	2.35 (0.10, 2.47)	1.10 (0.05)	2.28	5.10 (0.80, 6.34)	2.38 (0.37)	2.45	30 (22.83)	22 (20)	6.9
TiO_2	0.02	0.01 (0.003)	0.78	0.01 (0.00, 0.02)	0.01 (0.001)	1.20	0.02 (0.00, 0.03)	0.013 (0.002)	0.77	0.061 (0.047, 0.29)	0.048 (0.003)	0.90
Al_2O_3	0.49 (0.22, 0.80)	1.00	–	0.28 (0.09, 0.41)	1.00	–	0.59 (0.14, 0.76)	1.00	–	1.5 (1.1, 6.8)	1.0	
Fe_2O_3	0.18 (0.08, 0.35)	0.16 (0.07)	1.10	0.08 (0.04, 0.13)	0.07 (0.04)	0.85	0.15 (0.04, 0.19)	0.13 (0.04)	0.77	0.45 (0.29, 1.7)	0.43 (0.088)	0.79
FeO	0.13 (0.03, 0.15)	0.10 (0.02)	0.68	0.11 (0.02, 0.14)	0.09 (0.02)	0.94	0.13 (0.05, 0.20)	0.10 (0.04)	0.57			
MgO	0.37 (0.02, 0.12)	0.22 (0.02)	4.75	0.36 (0.03, 0.39)	0.22 (0.02)	7.63	0.38 (0.02, 0.40)	0.23 (0.01)	4.03	0.44 (0.17, 1.3)	0.40 (0.11)	2.2
CaO	53.58 (0.84, 54.513)	38.31 (0.60)	815	54.49 (0.26, 54.77)	38.96 (0.19)	1450	52.28 (0.68, 53.19)	37.38 (0.48)	663	36 (14, 48)	46 (24)	254
Na_2O	0.03 (0.01, 0.04)	0.02 (0.00)	0.63	0.02 (0.01, 0.03)	0.02 (0.004)	0.76	0.03 (0.00, 0.03	0.02 (0.002)	0.51	0.038 (0.10, 0.75)	0.038 (0.16)	0.29
K_2O	0.13 (0.03, 0.17)	0.11 (0.02)	1.21	0.09 (0.00, 0.10)	0.08 (0.02)	1.53	0.15 (0.02, 0.18)	0.13 (0.02)	1.20	0.42 (0.31, 1.9)	0.45 (0.050)	1.3
P_2O_5	0.03 (0.01, 0.04)	0.01 (0.00)	6.52	0.02 (0.01, 0.03)	0.01 (0.002)	7.27	0.03 (0.00, 0.04)	0.01 (0.002)	5.57	0.031 (0.014, 0.10)	0.020 (0.005)	2.5
MnO	0.07 (0.02, 0.124)	0.05 (0.02)	20.89	0.09 (0.01, 0.10)	0.07 (0.01)	44.39	0.06 (0.01, 0.07)	0.05 (0.005)	16.10	0.064 (0.026, 0.14)	848 (415)	8.8

analysis showed that the calcite content (92.68–99.19 wt%) is consistent with the calculations from the chemical analysis (91.06–97.22 wt%). Apart from the calcium, other major and trace elements are only present in low concentrations due to the diluting effect of the carbonate (Hu et al., 2009). The value of the Ti, Si, K, Na, and Fe average enrichment factors (listed in Table 2) for the Scaglia Rossa red limestone, the Scaglia Rossa white limestone, and the Scaglia Bianca white limestone are similar to the data reported by Turgeon and Brumsack (2006) from Scaglia Bianca, suggesting that both the Scaglia Rossa and the Scaglia Bianca have the same terrigenous origin.

Trace elements and proxy elements are also only present in very low concentrations (Hu et al., 2009). The low Mn content suggests dysoxic bottom-water conditions at the sediment/water interface (Landing and Bruland, 1980; Bruland, 1983; Landing and Bruland, 1987; Turgeon and Brumsack, 2006; Hu et al., 2009). Other proxy elements, such as Ni, Co, Cr, V and Ce are present in very low abundances: the average Ni/Co and V/Cr ratios are 0.7 and 3.2 in white limestone and 0.8 and 1.8 in red limestone. The delta Ce value ranges from 0.28–0.42, with an average of 0.34. These indices suggest that both the Scaglia Rossa white limestone and the Scaglia Bianca were deposited in dysoxic to oxic conditions, and that the red limestone was deposited in oxic to highly oxic conditions.

5.5. Mineralogical variation within the section

Quartz and boehmite have been identified as two major terrestrial minerals. Montmorillonite and illite were present as trace mineral residues, identified after dilute acetum dissolution. The absence of commonly found plagioclase, or other Fe or Mg bearing silicates suggests that the simple two-phase assemblage of minerals may have been transported from subtropical areas by seasonal north-easterly or easterly winds, and deposited simultaneously with the calcite precipitation, in a pelagic ocean environment. Boehmite is the major ore mineral in Mediterranean-type bauxite. This type of bauxite was usually found in a different geological time and was deposited in the Alpine ranges of Italy (Mongelli and Acquafredda, 1999), Austria, Hungary (Bárdossy and Bárdossy, 1984), Turkey (Öztürk et al., 2002) and France (Meyer, 2004). Thus the ancient Eurasian craton, located to the north or northeast of present day Italy, may have been the major detrital source area.

The distributions of the aluminous oxides and boehmite, the silica oxides and quartz, and the iron oxides in the Vispi Quarry section are shown in Figs. 7a,b and c respectively. The chemical data used was measured by XRF (Hu et al., 2009). The weight fractions for quartz and boehmite were determined by whole pattern fitting of the powder XRD results for the limestones, and the fitting was carried out using a GSAS programme (Larson and Von Dreele,

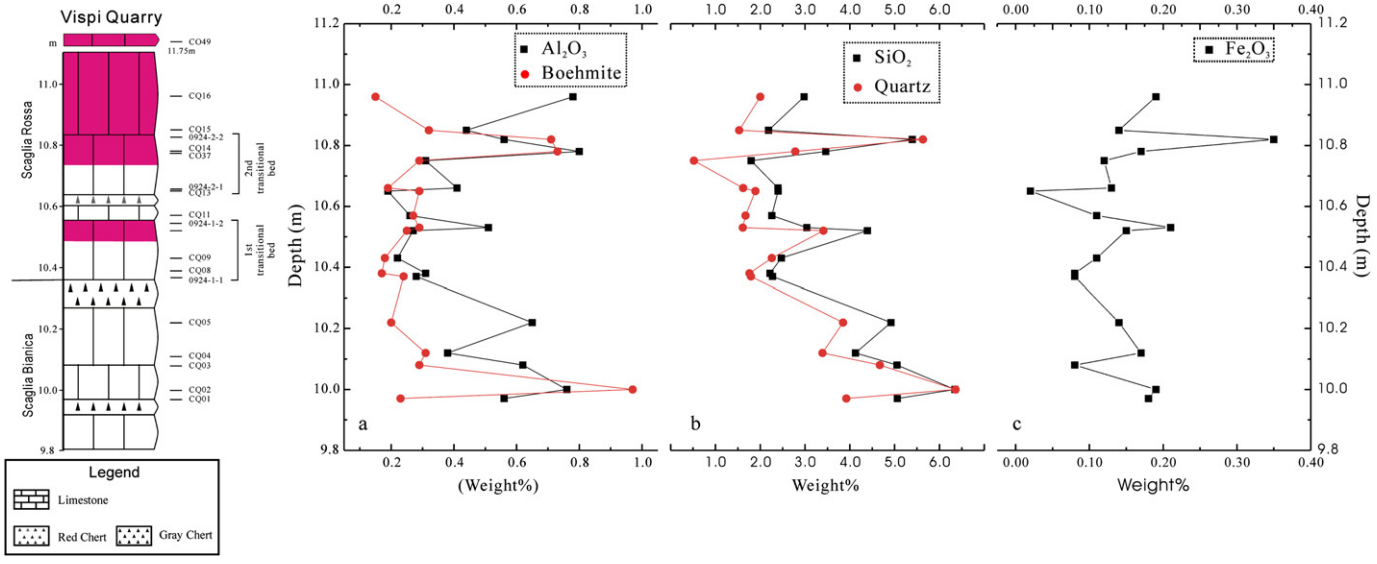

Fig. 7. Distribution of mineral components and chemical compositions in the Vispi Quarry section.

2004). Fig. 7 shows that all curves are consistent from the bottom to the top of the section. From the Scaglia Bianca to the Scaglia Rossa the iron oxide content varied together with the increase or decrease in aluminum oxide and silica oxide. The iron oxide content was, however, very low, with an average value of 0.22% in the Scaglia Rossa red limestone and 0.12% in the Scaglia Rossa and Bianca white limestones. The change in the quartz fraction within the section was consistent with the change in its SiO_2 chemical fraction. The average quartz content in total SiO_2 was 69.4% in the red limestone (8 samples) and 82.6% in the white limestones (9 samples), suggesting that the extra SiO_2 in the white limestones was from other silicate minerals, such as illite and montmorillonite. Because of the diluting effect of the carbonate, changes in these small fractions of Al_2O_3, SiO_2, and Fe_2O_3 followed similar trends from the Scaglia Bianca to the Scaglia Rossa limestones, suggesting that these oxides had the same origins. This suggestion is supported by the TFe_2O_3 and Al_2O_3 correlations which indicate that the iron oxide residues in the terrigenous minerals and the detrital source remained the same throughout the middle Turonian (Hu et al., 2009).

Fig. 7a shows that the distribution curves plotted from boehmite and Al_2O_3 were slightly different from each other. The lowest weight fraction of boehmite was in the pink limestone CQ-16, but the Al_2O_3 weight fraction was here at its highest, as were the quartz and Fe_2O_3 weight fractions. The weight fractions for boehmite were much smaller after refinement by GSAS, but much bigger according to their chemical data, suggesting that there is much amorphous material in the limestone. An accurate quantity can not be calculated for the amorphous material due to absence of a standard mineral, but it can be roughly evaluated by following formula: $Al_2O_{3\ amor.,\ wt} = Al_2O_{3\ chemi,\ wt} - 0.85 \times Boeh_{wt}$ where 0.85 was calculated by the molecular weight between the $0.5Al_2O_3$ and boehmite according to the aluminum mole fraction. Because of the higher degree of crystallization and much higher sensitivity to the XRD, the changes in the quartz content matched perfectly the changes in SiO_2 content within the section. Since the extremely strong absorption and the fluorescence radiation of iron exited by Cu Kα radiation, the detection limit for hematite is much higher than for quartz and boehmite. It was therefore impossible to obtain the hematite content directly from the whole pattern fitting of powder XRD patterns for carbonate samples when the iron oxide content was very low. Hence, only an iron oxide trend has been illustrated in Fig. 7c. This trend was similar to the trend for Al_2O_3 and SiO_2, which may suggest that the iron oxide had a similar origin to the quartz and boehmite.

6. Conclusions

(1) Manganese was incorporated into the structure of calcite to form a Mn^{2+}-bearing carbonate; the Mn^{2+} could have endowed the carbonate with a pink tinge.

(2) The iron content had both continental and oceanic origins. The ferric oxide or hematite had a continental origin and has been considered the most important pigment responsible for the red color in the limestone. The ferric oxide was imported into the ocean together with clay minerals such as boehmite and illite or montmorillonite.

(3) The boehmite and quartz, as well as minor montmorillonite and illite, were imported into the ocean during the precipitation of both the Scaglia Bianca white limestone and the Scaglia Rossa red limestone. However, minor hematite was also imported into the CORBs, along with the other detrital minerals, which suggests that the climate was different during the formation of these two different colored limestones. The climate on the paleo-continent during formation of the CORBs involved an alternation of warm, wet winters with hot dry summers, while the climate during formation of the COWBs was continuously warm and wet, with no hot dry summers.

(4) A terrigenous origin is proposed for the boehmite and quartz in the limestones. Boehmite was the most important ore mineral in Mediterranean-type bauxites and the product of intensive chemical weathering in a hot climate, deriving from the alteration of Fe-bearing aluminosilicates. It provides additional important evidence of a 'global greenhouse effect' during the Cretaceous.

(5) The presence of boehmite and its role in the coloring mechanism also suggest that the sedimentary records in the ocean reflect global climatic changes on the terrestrial continent during the Cretaceous.

Acknowledgements

We are grateful to Prof. Massimo Sarti for his support in the field. We are also deeply grateful to the reviewers of this paper for their constructive, valuable comments. This study was financially supported by the Chinese MOST 973 Project (2006CB701402). This paper is a contribution to the International Geosciences Project 555.

References

Alvarez, W., Arthur, M.A., Fisher, A.G., Lowrie, W., Napoleone, G., Premoli-Silva, I., Roggenthen, W.M., 1977. Upper Cretaceous-Paleocene magnetic stratigraphy at Gubbio, Italy, V. Type section for the Late Cretaceous-Paleocene geomagnetic reversal time scale. Geological Society of America Bulletin 88, 383–389.

Alvarez, W., Montanari, A., 1988. The Scaglia limestones (Late Cretaceous-Oligocene) in the north-eastern Apennines carbonate sequence: stratigraphic context and geological significance. In: Premoli-Silva, I., Coccioni, R., Montanari, A. (Eds.), The Eocene-Oligocene Boundary in the Marche-Umbria Basin (Italy). IUGS Special Publication, F.lli Aniballi Publishers, Ancona, pp. 13–30.

Arthur, M.A., 1976. Sedimentology of Gubbio sequence and its bearing on paleomagnetism. Memorie della Società Geologica Italiana 15, 9–20.

Arthur, M.A., Fischer, A.G., 1977. Upper Cretaceous-Paleocene magnetic stratigraphy at Gubbio, Italy, I. Lithostratigraphy and sedimentology. Geological Society of America Bulletin 88, 367–371.

Arthur, M.A., Premoli-Silva, I., 1982. Development of widespread organic carbon-rich strata in the Mediterranean Tethys. In: Schlanger, S.O., Cita, M.B. (Eds.), Nature and Origin of Cretaceous Carbon-Rich Facies. Academic Press, New York, pp. 1–54.

Bárdossy, A., Bárdossy, Gy, 1984. Comparison of geostatistical calculations with the results of open pit mining at the Iharkut bauxite district, Hungary: a case study. Mathematical Geology 16 (2), 173–191.

Bates, T.E., 1962. Halloysite and gibbsite formation in Hawaii. Clays and Clay Mineral 9, 315–328.

Baudin, F., Fiet, N., Coccioni, R., Galeotti, S., 1998. Organic matter characterization of the Selli Level (Umbria–Marche Basin, central Italy). Cretaceous Research 19, 701–714.

Bhattacharyya, T., Pal, D.K., Srivastava, P., 2000. Formation of gibbsite in the presence of 2:1 minerals: an example from Ultisols of northeast India. Clay Mineral 35, 827–840.

Bruland, K.W., 1983. Trace elements in sea-water. In: Riley, J.P., Chester, R. (Eds.), Chemical Oceanography, vol. 8. Academic Press, London, UK, pp. 157–220.

Cai, Y., Li, X., Pan, Y., Hu, X., 2008. The color-causing mechanism of Mn^{2+} and Fe^{3+}: evidence from the Italian Cretaceous pelagic red limestones. Acta Geologica Sinica 82 (1), 133–138.

Calderoni, G., Ferrini, V., 1984. Abundances and chemical fractionation of Al, Fe, Mn, Zn, Pb, Cu and Tl in Cretaceous-Palaeocence limestones from Gubbio (Central Italy). Geochemical Journal 18, 31–41.

Centamore, E., Fumanti, F., Nisio, S., 2002. The central-Northern Apennines geological evolution from Triassic to Neogene time. Bollettino della Societá Geologica Italiana 1, 181–197 (special volume).

Certini, G., Wilson, M.J., Hillier, S.J., Fraser, A.R., Delbos, E., 2006. Mineral weathering in trachydacitic-derived soils and saprolites involving formation of embryonic halloysite and gibbsite at Mt. Amiata, Central Italy. Geoderma 133, 173–190.

Channell, J.E.T., Freeman, R., Heller, F., Lowrie, W., 1982. Timing of diagenetic hematite growth in red pelagic limestones from Gubbio (Italy). Earth and Planetary Science Letters 58, 189–201.

Coccioni, R., 1996. The Cretaceous of the Umbria–Marche Apennines (central Italy). In: Wiedmann, J. (Ed.), Symposium "Cretaceous Stratigraphy, Paleobiology and Paleobiogeography". Tübingen, pp. 129–136.

Coccioni, R., Franchi, R., Nesci, O., Perilli, N., Wezel, F.C., Battistini, F., 1990. Stratigrafia, micropaleontologia e mineralogia delle Marne a Fucoidi delle sezioni di Poggio le Guaine e del Fiume Bosso (Appennino umbro–marchigiano). Atti 28 Convegno Internazionale bFossili, Evoluzione, AmbienteQ, Pergola, 25–30 ottobre 1987. Tecnostampa, 163–201.

Coccioni, R., Franchi, R., Nesci, O., Wezel, F.C., Battistini, F., Pallecchi, P., 1989. Stratigraphy and mineralogy of the Selli Level (early Aptian) at the base of the Marne a Fucoidi in the Umbro–Marchean Apennines, Italy. In: Wiedmann, J. (Ed.), Cretaceous of the Western Tethys. Proceedings 3rd International Cretaceous Symposium, Tfbingen 1987. E. Schweizerbart'sche Verlagsbuchhandlung, Stuttgart, pp. 563–584.

Coccioni, R., Galeotti, S., Ragni, D., 1992. Litho- and biostratigraphy of the Scaglia Bianca Formation (late Albian–late Cenomanian) in the Umbria–Marche Apennines (Italy). 6th Annual Meeting of IGCP 262 (Tethyan Creataceous Correlation)-Creataceous Facies in Orogenic Belts Athens, 22–26 May, 1992, pp.4.

Coccioni, R., Galeotti, S., Gravili, M., 1995. Latest Albian–early Turonian deep-water agglutinated foraminifera in the Bottaccione section (Gubbio, Italy)-Biostratigraphic and palaeoecology implications. Revista Española de Paleontologia, Numero Homenaje Al Dr. Guillermo Colom, 135–152.

Coccioni, R., Luciani, V., 2004. Planktonic foraminifera and environmental changes across the Bonarelli event (OAE2, Latest Cenomanian) in its type area: a high resolution study from the Tethyan reference Botaccioni section (Gubbio, central Italy). Journal of Foraminifera Research 34, 109–129.

Coccioni, R., Nesci, O., Tramontana, M., Wezel, F.C., Moretti, E., 1987. Descrizione di un livello-guida radiolaritico-bituminoso-ittiolitico alla base delle Marne a Fucoidi nell'Appennino umbro-marchigiano. Bollettino della Societá Geologica Italiana 106, 183–192.

D'Argenio, B., Mindszenty, A., 1995. Bauxites and related paleokarst: tectonic and climatic event markers at regional unconformities. Eclogae Geologicae Helvetiae 88, 453–499.

Deaton, B.C., Balsam, W.L., 1991. Visible spectroscopy: a rapid method for determining hematite and goethite concentration in geological materials. Journal of Sedimentary Research 61, 628–632.

Einsele, G., 1992. Sedimentary Basins - Evolution, Facies and Sediment Budget. Springer-Verlag, Berlin, pp. 628.

Eren, M., Kadir, S., 1999. Colour origin of upper cretaceous pelagic red sediments with the Eastern Pontides, Northeast Turkey. International Journal of Earth Sciences 88, 593–595.

Eren, M., Kadir, S., 2001. Colour genesis of Upper Cretaceous pelagic red sediments within the Eastern Pontides, NE Turkey. Yerbilimleri 24, 71–79.

Franke, W., Paul, J., 1980. Pelagic redbeds in the Devonian of Germany - deposition and diagenesis. Sedimentary Geology 25, pp. 231–256.

Furian, S., Barbiéro, L., Boulet, R., Curmi, P., Grimaldi, M., Grimaldi, C., 2002. Distribution and dynamics of gibbsite and kaolinite in an oxisol of Serra do Mar, southeastern Brazil. Geoderma 106, 83–100.

Gratziu, C., Schiaffino, L., 1967. Ricerche mineralogieche sulla "Scaglia Umbra", serie dei monti di Gubbio (Appennino Centrale). Atti della Società Toscana Scienze Naturali 74, 502–540.

Green, C.P., Eden, M.J., 1971. Gibbsite in the weathered Dartmoor granite. Geoderma 6, 315–317.

Habermann, D., Neuser, R.D., Richter, D., 1998. Low limit of Mn-activated cathodoluminescence of calcite: state of the art. Sedimentary Geology 116, 13–24.

Herrmann, L., Anongrak, N., Zarei, M., Schuler, U., Spohrer, K., 2007. Factors and processes of gibbsite formation in Northern Thailand. Catena 71, 279–291.

Hu, X., Chen, W.-B., Ji, J.F., 2009. Origin of Cretaceous Oceanic Red Beds from the Vispi Quarry Section, Central Italy: Visible Reflectance and Inorganic Geochemistry. SEPM Special Publication (Accepted).

Hu, X., Jansa, L., Sarti, M., 2006. Mid-Cretaceous oceanic Red Beds in the Umbria-Marche Basin, Central Italy: constraints on paleoceanography and palaeoclimate. Palaeogeography, Palaeoclimatology, Palaeoecology 233, 163–186.

Hu, X., Jansa, L., Wang, Ch., Sarti, M., Bak, K., Wagreich, M., Michalik, J., Sotak, J., 2005. Upper Cretaceous Oceanic Red Beds (CORB) in the Tethys: occurrence, lithofacies, age and environment. Cretaceous Research 26, 3–20.

ICDD, 2004. Powder Diffraction File 2. The International Centre for Diffraction Data.

Ji, J.F., Chen, J., Balsam, W., Liu, L.W., Chen, Y., Zhao, L., Zhou, W., 2007. Quantitative analysis of hematite and goethite in the chinese loess-paleosol sequences and its implication for dry and humid variability. Quaternary Sciences 27, 221–229 (In Chinese with English Abstract).

Jongmans, A.G., van Oort, F., Nieuwenhuyse, A., Buurman, P., Jaunet, A.M., van Doesburg, J.D.J., 1994. Inheritance of 2:1 phyllosilicates in Costa Rican andisols. Soil Science Society of America Journal 58, 494–501.

Kleber, M., Schwendenmann, L., Veldkamp, E., Rößner, J., Jahn, R., 2007. Halloysite versus gibbsite: silicon cycling as a pedogenetic process in two lowland neotropical rain forest soils of La Selva, Costa Rica. Geoderma 138, 1–11.

Kloprogge, J.T., Ruan, H.D., Frost, R.L., 2002. Thermal decomposition of bauxite minerals: infrared emission spectroscopy of gibbsite, boehmite and diaspore. Journal of Materials Science 37, 1121–1129.

Landing, W.M., Bruland, K.W., 1980. Manganese in the North Pacific. Earth and Planetary Science Letters 49, 45–56.

Landing, W.M., Bruland, K.W., 1987. The contrasting biogeochemistry of iron and manganese in the Pacific Ocean. Geochimica et Cosmochimica Acta 51, 29–43.

Larson, A.C., Von Dreele, R.B., 2004. General Structure Analysis System (GSAS), Los Alamos National Laboratory Report LAUR 86–748.

Li, J., Zhang, J., Zhao, D., Lü, Y., Shen, D., Fan, X., 2006. Effects of Mn content on structure and Photoluminescence of ZnO Nano films. Chinese Journal of Liquid Crystals and Displays 21, 615–619 (In Chinese with English Abstract).

Lowrie, W., Alvarez, W., 1977. Paleomanetic studies of the Scaglia Rossa limestone in Umbria. Memorie della Società Geologica Italiana 15, 41–50.

Lowrie, W., Alvarez, W., Asaro, F., 1990. The origin of the white beds below the Cretaceous-Tertiary boundary in the Gubbio section, Italy. Earth and Planetary Science Letters 98, 303–312.

Luterbacher, H.P., Premoli-Silva, I., 1962. Note preliminaire sur une revision du profil de Gubbio, Italie. Rivista Italiana di Paleontologia e Stratigrafia 68, 253–288.

Macedo, Z.S., Valerio, M.E.G., de Lima, J.F., 1999. Thermoluminescence mechanism of Mn^{2+}, Mg^{2+} and Sr^{2+} doped calcite. Journal of Physics and Chemistry of Solids 60, 1973–1981.

Marchegiani, B.G., Cello, G., Deiana, G., Mazzoli, S., Tondi, E., 1999. Pre-orogenic tectonics in the Umbria–Marche sector of the Afro-Adriatic continental margin. Tectonophysics 315, 123–143.

Medlin, W.L., 1963. Emission centers in thermoluminescent calcite, dolomite, magnesite, aragonite, and anhydrite. Journal of the Optical Society of America 53 (11), 1276–1284.

Mehta, S.K., Kalsotra, A., 1991. Kinetics and hydrothermal transformation of gibbsite. Journal of Thermal Analysis and Calorimetry 37, 267–275.

Meyer, M.H., 2004. Availability of bauxite reserves. Natural Resources Research 13 (3), 161–172.

Mongelli, G., Acquafredda, P., 1999. Ferruginous concretions in a Late Cretaceous Karst bauxite: composition and conditions of formation. Chemical Geology 158, 315–320.

Mulyanto, B., Stoops, G., Van Ranst, E., 1999. Precipitation and dissolution of gibbsite during weathering of andesitic boulders in humid tropical West Java, Indonesia. Geoderma 89, 287–305.

Nieuwenhuyse, A., 1996. Landscape Formation and Soil Genesis in Volcanic Parent Materials in Humid Tropical Lowlands of Costa Rica. PhD thesis, Wageningen University, Wageningen, The Netherlands.

Öztürk, H., Hein, J.R., Hanilçi, N., 2002. Genesis of the Dogankuzu and Mortas, bauxite deposits, Taurides, Turkey: separation of Al, Fe, and Mn and implications for passive margin metallogeny. Economic Geology 97, 1063–1077.

Perić, Z., Krstulović, R., Vućak, M., 1996. Investigation of dehydroxylation of gibbsite into boehmite by DSC analysis. Journal of Thermal Analysis and Calorimetry 46, 1339–1347.

Premoli-Silva, I., 1977. Upper Cretaceous-Paleocene magnetic stratigraphy at Gubbio, Italy, II. Biostratigraphy. Geological Society of America Bulletin 88, 371–374.

Premoli-Silva, I., Paggi, L., Monechi, S., 1977. Cretaceous through Paleocene biostratigraphy at the pelagic sequence at Gubbio, Italy. Memorie della Società Geologica Italiana 15, 21–32.

Premoli-Silva, I., Sliter, W.V., 1994. Cretaceous planktonic foraminiferal biostratigraphy and evolutionary trends from the Bottaccione section, Gubbio, Italy. Paleontolographia Italica 82, 1–89.

Putnis, A., Hinrichs, R., Putnis, C.V., Golla-Schindler, U., Collins, L.G., 2007. Hematite in porous red-clouded feldspars: evidence of large-scale crustal fluid–rock interaction. Lithos 95, 10–18.

Pye, K., 1983. Red Beds. In: Goudie, A.S., Pye, K. (Eds.), Chemical Sediments and Geomorphology. Academic Press, London, pp. 227–263.

Renz, O., 1936. Stratigraphische und mikropalaeontolische Untersuchung der Scaglia (Obrere Kreide-Tertiar) im zentralen Apennin. Eclogae Geologicae Helvetiae 29, 1–149.

Samuel, N., Bruno, D., 2003. Coexistence of allophane, gibbsite, kaolinite and hydroxy-Al-interlayered 2:1 clay minerals in a perudic Andosol. Geoderma 117, 203–214.

Schlanger, S.O., Jenkyns, H.C., 1976. Cretaceous anoxic events: causes and consequences. Geologie en Mijnbouw 55, 179–184.

Sighinolfi, G.P., 1981. The problem of Cretaceous-Tertiary boundary event. Preliminary geochemical investigations on the Scaglia Rossa formation (Centra Italy). Periodico di Mineralogia 50, 91–111.

Torrent, J., Schwertmann, U., 1987. Influence of hematite on the color of Red Beds. Journal of Sedimentary Petrology 57, 682–686.

Tremolada, F., 2002. Aptian to Campanian calcareous nannofossil biostratigraphy from the Bottaccione section, Gubbio, central Italy. Rivista Italiana di Paleontologia e Stratigrafia 108, 441–456.

Trolard, F., Tardy, Y., 1987. The stabilities of gibbsite, boehmite, aluminous goethites and aluminous hematites in bauxites, ferricretes and laterites as a function of water activity, temperature and particle size. Geochimica et Cosmochimica Acta 51, 945–957.

Turgeon, S., Brumsack, H.J., 2006. Anoxic vs. dysoxic events reflected in sediment geochemistry during the Cenomanian-Turonian Boundary Event (Cretaceous) in the Umbria-Marche Basin of central Italy. Chemical Geology vol. 234, 321–339.

Turner, P., 1980. Continental Red Beds. Elsevier, Amsterdam, pp. 562.

Van Houten, F.B., 1973. Origin of Red Beds: a review-1961–1972. Annual Review of Earth and Planetary Sciences 1, 39–61.

Vannucci, S., Vannucci, R., Mazzuccottelli, A., Faranchi, R., 1979. Risultati preliminary dello studio petrografico e geochimico della Scaglia Bianca e della Scaglia Rossa della sezione del Bottaccione (Gubbio). Ateneo Parmense Acta Naturalia 15, 261–266.

Wada, K., Aomine, S., 1966. Occurrence of gibbsite in weathering of volcanic materials at Kuroishibaru, Kumamoto. Soil Science & Plant Nutrition 12 (4), 25–31.

Wezel, F.C., 1979. The Scaglia Rossa Formation of central Italy: results and problems emerging from a regional study. Ateneo Parmense Acta Naturalia 15, 243–259.

Wilke, B.M., Schwertmann, U., 1977. Gibbsite and halloysite decomposition in strongly acid podzolic soils developed from granitic saprolite of the Bayerischer Wald. Geoderma 19, 51–61.

Yilmaz, I.ö, 2008. Cretaceous pelagic Red Beds and black shales (Aptian-Santonian), NW Turkey: global oceanic anoxic and oxic events. Turkish Journal of Earth Sciences 17, 263–296.

Zhang, Z., Hua, R., Ji, J., Cai, Y., 2005. Spectrographic characteristics of calcite formed at different mineralization stages in xiazhuang uranium ore field. Acta Mineralogica Sinica 25, 33–38.

Ziegler, K., Hsieh, J.C.C., Chadwick, O.A., Kelly, E.F., Hendricks, D.M., Savin, S.M., 2003. Halloysite as a kinetically controlled end product of arid-zone basalt weathering. Chemical Geology 202, 461–478.